Band nesting in two-dimensional crystals: an exceptionally sensitive probe of strain

Lukas Mennel,[*,†,¶] Valerie Smejkal,[*,‡,¶] Lukas Linhart,[‡] Joachim Burgdörfer,[‡] Florian Libisch,[‡] and Thomas Mueller[†]

†*Vienna University of Technology, Institute of Photonics, Gußhausstraße 27-29, 1040 Vienna, Austria, EU*

‡*Vienna University of Technology, Institute of Theoretical Physics, Wiedner Hauptstraße 8-10, 1040 Vienna, Austria, EU*

¶*These authors contributed equally to this work.*

E-mail: lukas.mennel@tuwien.ac.at; valerie.smejkal@tuwien.ac.at

Abstract

Band nesting occurs when conduction and valence bands are approximately equispaced over regions in the Brillouin zone. In two-dimensional materials band nesting results in singularities of the joint density of states and thus in a strongly enhanced optical response at resonant frequencies. We exploit the high sensitivity of such resonances to small changes in the band structure to sensitively probe strain in semiconducting transition metal dichalcogenides (TMDs). We measure and calculate the polarization-resolved optical second harmonic generation (SHG) at the band nesting energies and present the first measurements of the energy-dependent nonlinear photoelastic effect in atomically thin TMDs (MoS_2, $MoSe_2$, WS_2, and WSe_2) combined with a theoretical analysis of the underlying processes. Experiment and theory are found to be in good qualitative agreement displaying a strong energy dependence of the SHG, which can

be exploited to achieve exceptionally strong modulation of the SHG under strain. We attribute this sensitivity to a redistribution of the joint density of states for the optical response in the band nesting region. We predict that this exceptional strain sensitivity is a general property of all 2D materials with band nesting.

Keywords

band nesting, uniaxial strain, second harmonic generation, TMDs, two-dimensional

Introduction

The unique electronic, optical, and mechanical properties of atomically thin crystals continue to attract considerable interest motivated in part by both fundamental aspects of low-dimensional physics and future technological applications. The novel properties of these two-dimensional (2D) materials constitute a versatile playground for material science and provide new opportunities for device development. One of their outstanding physical properties is the strong electron-photon interaction: a single transition metal dichalcogenide (TMD) monolayer can absorb up to 20% of light in the spectral region of the so-called C-exciton.[1] This strong absorption is attributed to singularities at critical points in the joint density of states (JDOS) whose signature are nearly constant energy spacings between the conduction and the valence bands that vary little over extended regions of the Brillouin zone, an effect also known as band nesting.[2,3]

In addition to strong photoabsorption, atomically thin crystals exceed their bulk counterparts also in their high tolerance to strain. While bulk silicon breaks at around 1.5% strain,[4] 2D crystals can sustain extremely high levels of strain[5] of up to 25%. Strain strongly changes material properties enabling strain engineering to tailor device properties:[6] homogeneous strain in TMDs modulates the bandgap,[7] softens or hardens phononic modes,[8] and changes the electron-phonon-coupling.[9] Even more intriguing effects appear in inhomoge-

neously strained 2D materials: pseudomagnetic fields emerge in graphene,[10] excitons funnel along strain gradients,[11] and single-photon emitters form in WSe_2 and WS_2.[12–17] While some devices such as highly efficient solar cells[18] and single photon sources[19] exploiting inhomogeneous strain have been proposed or already realized, many of the above effects still remain to be fully explored.

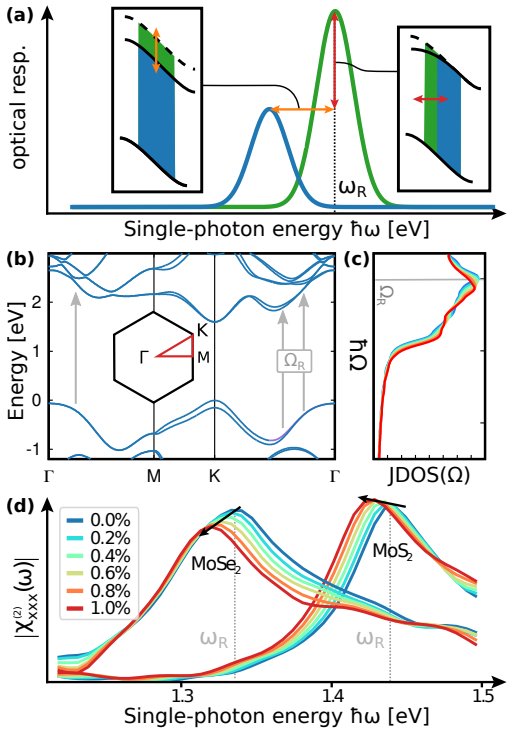

Figure 1: a) Band nesting leads to a peak in the optical response at resonance frequency $\omega_R = \Omega_R/n$. Left: bond stretching lowers ω_R. Right: deformation of bonds changes the absorption strength and width. b) Band structure and c) strained joint density of states JDOS(Ω) of MoS_2. d) Calculated second harmonic response $|\chi^{(2)}_{xxx}(\omega)|$ in armchair-direction of MoS_2 and $MoSe_2$ under varying uniaxial tensile strain.

Previous investigations have emphasized the effect of strain on the lower-lying A and B excitons in 2D semiconductors near band maxima or minima at the K point.[20–23] For some materials, recent studies found a high strain sensitivity at a fixed energy close to the C-exciton using second harmonic generation (SHG),[24,25] a nonlinear process where two photons of frequency ω are converted into one photon of frequency 2ω. However, little is known about the strain-dependence of the band nesting resonance.

In this letter we provide the first microscopic explanation for the strong strain dependence of SHG in two-dimensional semiconductors for which, until now, only phenomenological descriptions are available.[24] We identify band nesting as the origin of the extraordinary strain sensitivity, and thus provide the means to optimize strain sensitivity by probing at the appropriate resonant energies. Our results demonstrate that the impact of band nesting on the light-matter interaction in two-dimensional materials can be of similar importance as the well-known enhanced excitonic interaction. We verify our approach by measuring and simulating the second-order response of four different semiconducting TMDs MX_2 (M=Mo,W; X=S,Se) around the band nesting energies. The good qualitative agreement between theory and experiment found lends support to the proposed scenario governing the strain dependence. We expect our findings to be valid for any order of optical response and any 2D material featuring a band-nesting region.

Strain dependence of the optical susceptibility

The n^{th}-order optical response to a monochromatic light field with frequency ω is given by the susceptibility tensor $\chi^{(n)}_{ij_1\cdots j_n}(\omega)$, where $ij_1\cdots j_n$ denote cartesian directions. It is intimately connected to the joint density of states $\text{JDOS}(\Omega) \propto \sum_{C,V}\int_{\text{BZ}}\delta\left(\varepsilon_C(\mathbf{k})-\varepsilon_V(\mathbf{k})-\hbar\Omega\right)d\mathbf{k}$. The JDOS is a measure of accessible transitions at frequency Ω between the valence (V) and the conduction (C) bands with dispersion relation $\varepsilon_V(\mathbf{k})$ and $\varepsilon_C(\mathbf{k})$ [Fig. 1(b,c)]. Both the linear susceptibility $\chi^{(1)}_{ij}(\omega)$ as well as higher-order response functions are proportional to the JDOS, specifically

$$\chi^{(n)}_{ij_1\cdots j_n}(\omega) \propto \text{JDOS}(\Omega = n\omega) \tag{1}$$

[see Supporting Information (SI)]. Band nesting appears when the valence and the conduction bands run in parallel over an extended region in the Brillouin zone enhancing the number of state pairs between which transitions at a given frequency Ω_R thereby become

possible. In two dimensions, this results in singularities in the JDOS at such frequencies Ω_R leading to resonant enhancement of the optical response $\chi^{(n)}_{ij_1\cdots j_n}(\omega)$ when $n\omega = n\omega_R \equiv \Omega_R$. Finite lifetimes of the states and closely spaced neighbouring resonances lead to a finite width of the resonance in the optical response.

Upon straining a 2D crystal two effects appear near resonances due to band nesting: (I) bond stretching may reduce the energy difference between conduction and valence bands, reducing ω_R [left inset of Fig. 1(a)], and (II) the deformation of bonds will affect the peak height and width [right inset of Fig. 1(a)]. A combination of the two effects results in a substantial material- and energy dependent change of the optical response with strain when the second harmonic of the driving laser is resonant with the band nesting energies $2\omega = 2\omega_R$.

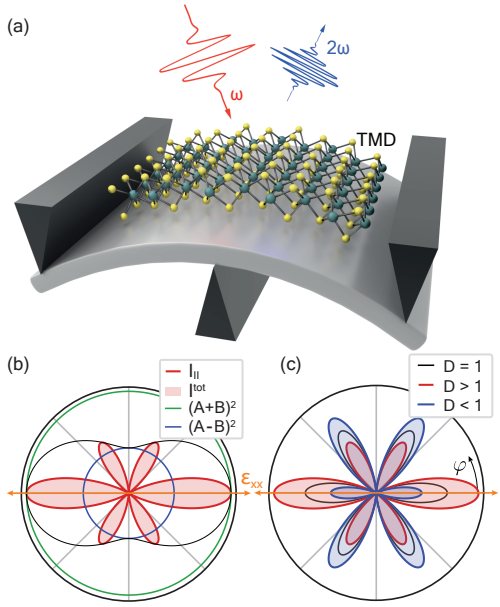

Figure 2: (a) Illustration of the three-point bending technique and SHG process. Polar plots of the SHG signal $I^{(2)}_{||}(\varphi)$ emitted with polarization collinear to the polarization of the driving laser with strain ϵ_{xx} in x-direction: (b) typical angular resolved SHG signal (red) together with the envelope function (black) with its extrema $(A \pm B)^2$ (green/blue) and the total intensity (red area) I^{tot}. c) SHG for different values of the distortion D.

To identify such a response in our experiments, we will focus on the second-harmonic generation (SHG) by a laser of frequency ω described by $\chi^{(2)}_{ijk}(\omega)$ which is strongly enhanced by band nesting.[26] The advantages of using SHG are that it is very sensitive to inversion

symmetry breaking and that driver and signal can easily be distinguished in the experiment since the response is measured at a frequency different from the driving frequency. As an example of the strain response as described above we consider the evolution of the x-component $\chi^{(2)}_{xxx}(\omega)$ of the second harmonic tensor under strain at fixed ω for different TMDs, see Fig. 1(d): (I) tensile strain reduces ω_R, red-shifting the peak and increasing (decreasing) $|\chi^{(2)}_{xxx}(\omega)|$ for $\omega < \omega_R$ ($\omega > \omega_R$). By contrast, (II) the change in resonance height (and width) is material specific: for $MoSe_2$, a decrease of the amplitude $|\chi^{(2)}_{xxx}(\omega)|$ with increasing strain reduces $|\chi^{(2)}_{xxx}(\omega)|$ on both sides of the resonance. Both effects combined lead to a strong decrease of $|\chi^{(2)}_{xxx}(\omega)|$ on the falling slope of the band nesting resonance ($\omega < \omega_R$), while there is almost no change in the response on the rising slope. Conversely, for MoS_2, the amplitude $|\chi^{(2)}_{xxx}(\omega_R)|$ increases with strain yielding a prominent increase of $|\chi^{(2)}_{xxx}(\omega)|$ with strain for frequencies below the band nesting resonance. We find similar systematics for the other tensor components of $\chi^{(2)}_{ijk}$ [see SI]. A high strain sensitivity of the SHG signal thus emerges on the rising or falling slopes of band nesting peaks giving an intuitive understanding of how the sensitivity of strain measurements using SHG can be optimized by choosing a suitable ω.

We use the symmetries of the crystal to reduce the description of the strained TMD crystal from the susceptibility tensor to two parameters which we will refer to in the remainder of the discussion. The SHG signal in the pristine TMD monolayers follows the $P\bar{6}m2$ space group (point group D_{3h}). The SHG signal emitted with polarization collinear to the polarization of the incoming laser as a function of the polarization angle φ ($\varphi = 0$ defines the x-direction) features a sixfold pattern in the strain dependent second harmonic intensity $I^{(2)}_{||}(\varphi) \propto \cos\left(3(\varphi - \delta)\right)^2$, where δ defines the armchair direction of the hexagonal lattice relative to $\varphi = 0$. The maxima correspond to the armchair directions $(\varphi - \delta) = 2n\pi/6$, $n = 0 \ldots 5$ (with maximally broken inversion symmetry) while the intensity vanishes along the zigzag directions $(\varphi - \delta) = (2n+1)\pi/6$ [Fig. 2(b)] for which inversion symmetry prevails. Uniaxial strain distorts the angle-dependence of the SHG intensity. It can be described in

terms of the parameters A and B giving the strength of the D_{3h} symmetry-preserving (A) and the symmetry-broken (B) contribution to the intensity[24,25]

$$I_{||}^{(2)}(\varphi) \propto \left(A(\overline{\overline{u}})\cos\left(3(\varphi-\delta)\right) + B(\overline{\overline{u}})\cos\left(2\theta+\varphi-3\delta\right)\right)^2, \tag{2}$$

where θ gives the strain direction relative to $\varphi = 0$ and $\overline{\overline{u}}$ is the strain tensor. We parameterize the effect of symmetry-breaking strain on SHG by two new parameters

$$I^{\text{tot}} = \int I_{||}(\varphi)d\varphi = \pi(A^2+B^2), \tag{3a}$$

$$D = \frac{(A+B)^2}{(A-B)^2}\ . \tag{3b}$$

The total intensity of the emitted SHG signal I^{tot} [Fig. 2(b)] gives the peak shape of the second harmonic signal. The distortion D is the ratio of the extremal values of the envelope function of the SHG $(A \pm B)^2$. It reflects the degree of symmetry breaking and can be used as a measure for the sensitivity of the SHG to strain. $D > 1$ ($D < 1$) if the envelope of the intensity in strain direction $(A+B)^2$ is larger (smaller) than in the orthogonal direction $(A-B)^2$ [see Eqs. (3) and Fig. 2(b,c)].

Results and discussion

To explore the sensitivity of the band nesting region in 2D materials to strain we measure and calculate the energy and strain dependent SHG in the four prominent semiconducting TMDs MoS_2, $MoSe_2$, WS_2 and WSe_2. We apply uniaxial strain to a monolayer and record the second harmonic intensity $I_{||}^{(2)}$ emitted with polarization collinear to the polarization of a linearly polarized laser with energies tunable around the C-exciton [Fig. 2(a)]. In the accompanying simulation we calculate the second-order harmonic tensor,[27] with energies and dipole matrix elements derived from DFT.[28] In Fig. 3 we present the wavelength and strain dependent results for MoS_2 ($D > 1$) and $MoSe_2$ ($D < 1$). We restrict our discussion to those

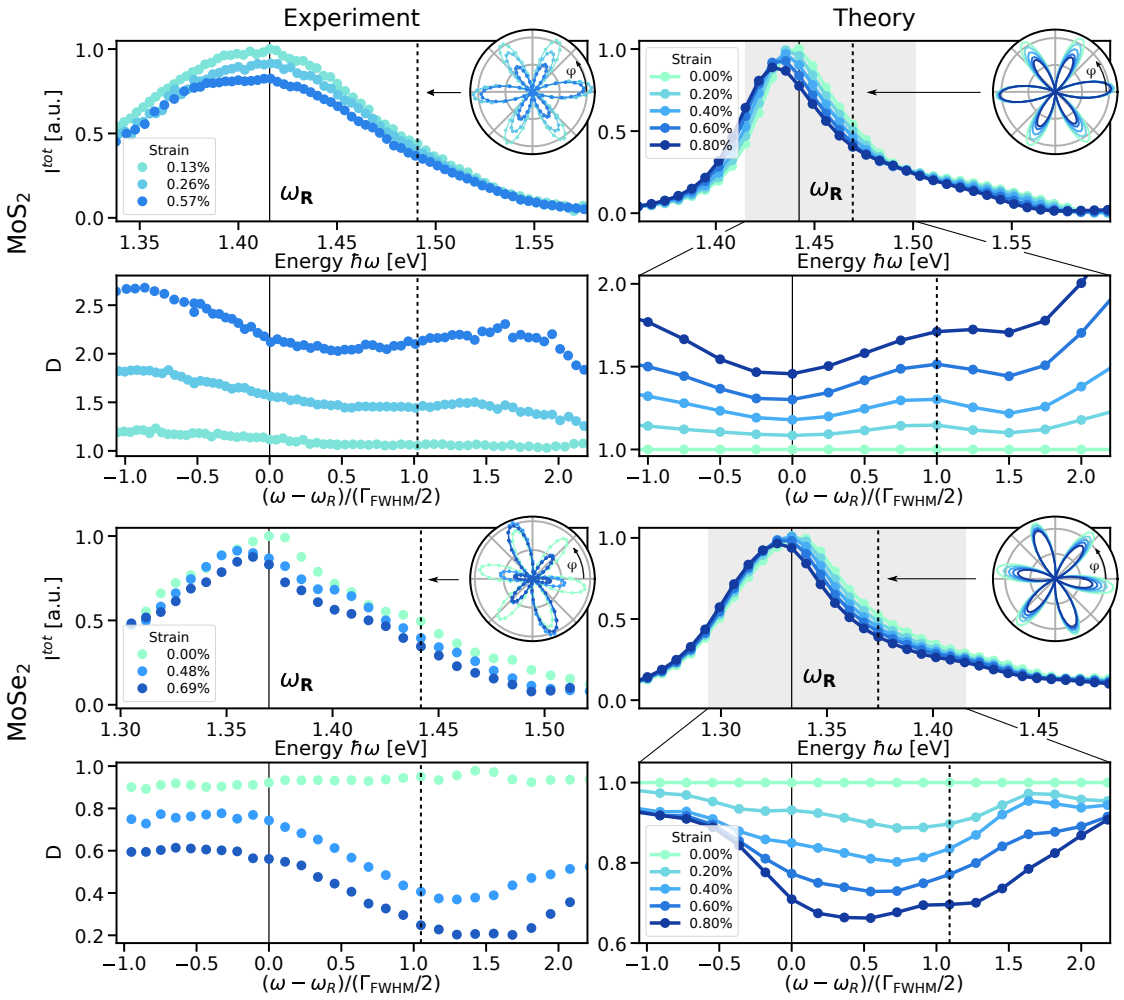

Figure 3: Experimental (left) and theoretical (right) total SHG intensity $I^{\mathrm{tot}} = \pi(A^2 + B^2)$ and distortion $D = (A+B)^2/(A-B)^2$ for MoS_2 (top) and $MoSe_2$ (bottom) at measured and calculated strain values (see legend). Solid vertical lines mark the resonance frequency $\omega_R = \Omega_R/2$. D is plotted in the vicinity of ω_R in scaled units (shaded area in theory shows the corresponding energy range, for the experimental data the energy scale and peak width scale coincide). The insets show one typical angular resolved SHG signal at an energy where strain has a large effect (marked by dashed vertical line), with $\varphi = 0$ fixed to the direction of strain (see SI for data at additional energies). Different lattice orientations w.r.t. the direction of strain result in rotated and deformed angular resolved patterns.

two materials for the sake of brevity, results for WS_2 and WSe_2 showing a similar behavior to MoS_2 can be found in the SI (Fig. S1).

We find good qualitative agreement between theory [Fig. 3, right column] and experiment [Fig. 3 left column]. Uniaxial strain leads to an energy dependent distortion that strongly affects the second-order response for all investigated TMDs. The distortion monotonically and substantially increases with strain showing the increasing degree of symmetry breaking of the strained lattice. The measured distortion for MoS_2 reaches maximal values of $D = 2.5$ at a strain of $\approx 0.6\%$ leading to a strongly distorted angle resolved polarization response as shown in the circular insets of Fig. 3. $MoSe_2$ also shows a strongly distorted angle resolved polarization response, yet we find a distortion $D < 1$. Both results confirm that strain has a particularly strong influence on the optical response in the band nesting region.

While our simulations are capable of reproducing the experimentally observed overall response of the SHG to strain, there remain some differences between theory and experiment: (i) the structures as a function of ω observed in both I^{tot} and D are considerably broader in the experiment than in theory (compare the peak width in SHG intensity in Fig. 3). We attribute this to interaction-induced broadening where temperature effects play an important role. The experiment was conducted at room temperature whereas the calculations assume 0 K and therefore neglect broadening due to electon-phonon interactions.[29] (ii) There is a shift between the resonant frequencies $\omega_R = \Omega_R/2$ in experiment and theory, in line with the well-known shortcoming of DFT in predicting conduction band energies in semiconductors[30] (see SI for a more detailed discussion). Changing the frequency axis to the dimensionless universal frequency scale near a resonance, $(\omega - \omega_R)/(\Gamma_{\mathrm{FWHM}}/2)$, allows for a qualitative comparison of the evolution of the distortion with strain around the C-exciton resonance between experiment and theory (see distortion plots in Fig. 3). (iii) The absolute magnitude of the distortion is underestimated in the calculation. We attribute this partly to the underestimation of elastic properties in DFT.[31] Additionally, the renormalization of the peaks with strain might be stronger when corrections from the electron-hole interactions via the

Bethe-Salpeter equation are included. Nevertheless, the overall evolution of the distortion with strain is very well captured within DFT and perturbation theory.

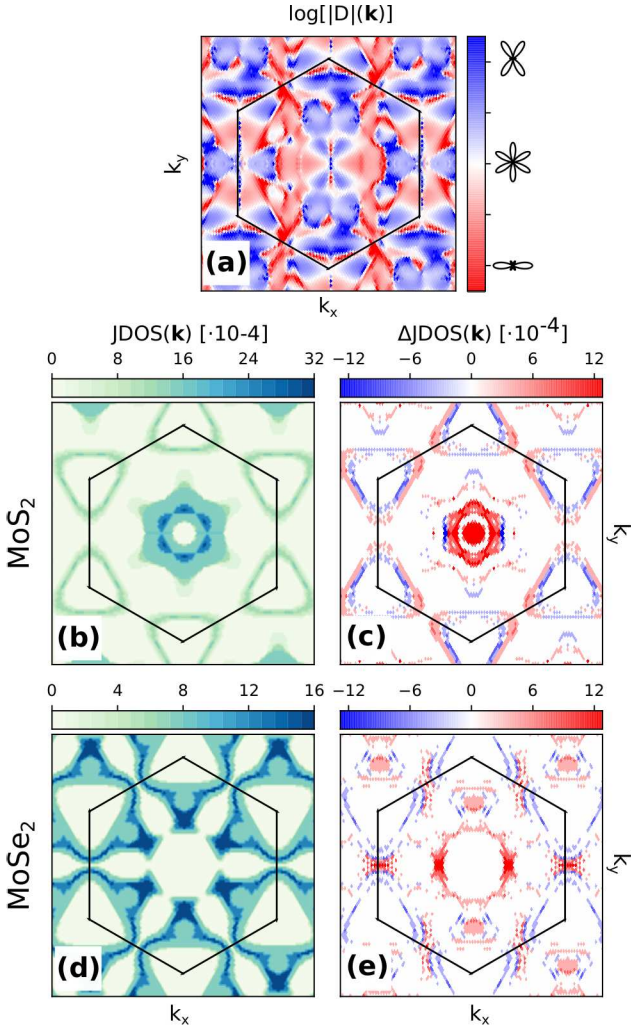

Figure 4: Brillouin zone resolved analysis. (a) The distortion distribution in unstrained MoS_2. (b, d) The JDOS(ω) of the unstrained crystal and (c, e) the change of the JDOS with 1% strain for MoS_2 and $MoSe_2$ at the energy of the maximum of $\chi^{(2)}$. While the peak of the JDOS(ω) in MoS_2 is localized around Γ (dark area corresponds to strong weight), a large fraction of the Brillouin zone is involved for $MoSe_2$. For details see text.

Comparing the optical response to strain of MoS_2 and $MoSe_2$ [top and bottom row in Fig. 3], the intensities I_{tot} [Eq. 3a] display similar trends while the evolution of the distortion D [Eq. 3b] with strain exhibits a striking qualitative difference: starting from a pristine value of $D = 1$, the value increases (decreases) with strain for MoS_2 ($MoSe_2$). To understand this difference we analyze the distribution of resonances within the Brillouin zone (BZ) and their

evolution with strain. The **k**-resolved contributions to the distortion $D(\mathbf{k})$ of the SHG [Fig. 4(a)] varies strongly over the BZ even for the unstrained material. The contributions of D for different **k** to the integrated distortion are weighted by the JDOS(**k**) which peaks in the band nesting regions. Without strain, those areas average out when integrating over the full BZ and lead to a symmetric response. Fig. 4(b-e) shows the JDOS(ω) and the change of the JDOS(ω) induced by 1% strain at the energy of the SHG-intensity maximum in the unstrained case. In MoS_2 the maximal band nesting is found in the vicinity of the Γ point [Fig. 4(b)] while for $MoSe_2$ it is more delocalized [Fig. 4(d)] with the major contribution along the $\Gamma - K$-line. These are also the areas reacting most strongly – yet qualitatively differently – to strain [Fig. 4(c,e)]. This results in the qualitatively different behavior of the two materials under strain, in line with our experimental and theoretical findings. Therefore differences in strain-induced distortions can be clearly attributed to the different location and extension of the band nesting region in reciprocal space.

Finally, let us assess the sensitivity of strain measurements using polarization resolved SHG and compare it with two common strain measurement techniques, Raman spectroscopy [8] and photoluminescence (PL).[9] As figure of merit we use the relative accuracy δ_X/σ_X of the corresponding observable X given by the ratio of the strain induced shift δ_x to the variance σ_x of this observable. In MoS_2, uniaxial tensile strain of 0.1 percent shifts the A-exciton peak[9] in PL with width $\sigma_A \approx 65\,\mathrm{meV}$ by $\delta_A = -2.8\,\mathrm{meV}$. The E^1_{2g} Raman peak[8] with width $\sigma_{2g} = 5\,\mathrm{cm}^{-1}$ is shifted by $\delta_{2g} = -0.21\,\mathrm{cm}^{-1}$. By comparison, the same strain results in a relative intensity variation $\delta I = (I^{\mathrm{env}}_{\parallel} - I^{\mathrm{env}}_{\perp})/I^{\mathrm{env}}_{\parallel} = 12.5 \times 10^{-2}$ with a width of $\sigma_I = 3.6 \times 10^{-2} I^{\mathrm{env}}_{\parallel}$ at an excitation wavelength of 895 nm, where $I^{\mathrm{env}}_{\parallel} \propto (A+B)^2$ and $I^{\mathrm{env}}_{\perp} \propto (A-B)^2$. The resulting relative accuracies $\delta_A/\sigma_A \approx \delta_{2g}/\sigma_{2g} \approx 0.04$ compared to $\delta_I/\sigma_I \approx 3.5$ illustrate the exceptional sensitivity of SHG. Thus, even small strains can be determined with SHG while measurements with Raman or PL would be challenging.

Conclusions

We present the first combined experimental and theoretical study exploring the sensitivity of the band nesting region in 2D crystals to strain. Strain sensitivity can be maximized by exploiting band nesting resonances. We determine the second-order harmonic response of four different transition metal dichalcogenides. The importance of the position of the band nesting region in the Brillouin zone is prominently displayed by the very different response of $MoSe_2$ to strain as opposed to MoS_2, WS_2 and WSe_2. A similar energy and strain dependence should also be visible in other optical processes and for other 2D crystals featuring band nesting.

Methods

Second harmonic generation measurements

To measure strain dependent SHG, we transfer mechanically exfoliated TMD monolayers onto flexible polyethylene naphthalate (PEN) substrates covered in hardbaked SU-8 (MicroChem) and subsequently encapsulate the TMD crystal with polycarbonate (PC). Uniaxial strain is applied by three-point bending of the flexible substrate which transfers the applied strain to the monolayer [see schematic in Fig. 2(a)]. A tunable Ti:sapphire laser delivers 200 fs pulses which are then circularly polarized. With a linear polarizer mounted on a rotation stage we choose a linear polarization along an angle φ. We focus the laser beam onto the TMD monolayer and collect the frequency doubled light in a backscattering geometry. The SHG response is then passed through the same linear polarizer and, after separation from the fundamental frequency, detected with a silicon amplified photodetector. For a polarization-resolved SHG measurement the linear polarizer is rotated by a full turn while measuring the intensity.

DFT and perturbation theory

To simulate SHG in TMDs, we first calculate the ground state electronic structure using all-electron density functional theory (DFT) as implemented in the exciting-code[28] with the PBE exchange-correlation-functional[32] including spin-orbit coupling. We apply strains up to 1% along the x-direction (armchair) of the crystal and relax the atoms and the cell in y-direction (zig-zag). To correct for the band gap underestimated in DFT we apply a scissor correction to match the band gap with the experimental position of the A-exciton[33] [see SI for details].

We calculate the second-order susceptibility $\chi^{(2)}_{ijk}$ applying a perturbative treatment to second order in the external field.[27] The expression for the second-order susceptibility $\chi^{(2)}_{ijk}(-2\omega,\omega,\omega)$ is given by (Eq. 35 in[27])

$$\chi^{(2)}_{ijk}(-2\omega,\omega,\omega) = \frac{e^3}{\omega^3\hbar m^2 V}\sum_{\mathbf{k}}\sum_{nml}\frac{G^{ijk}_{nml}(\mathbf{k})}{[\omega_{mn}(\mathbf{k})-2\omega]}\left[\frac{f_{nl}(\mathbf{k})}{\omega_{ln}(\mathbf{k})-\omega}+\frac{f_{ml}(\mathbf{k})}{\omega_{ml}(\mathbf{k})-\omega}\right], \quad (4)$$

where $G^{ijk}_{nml}(\mathbf{k}) = \frac{1}{2}\mathrm{Im}\left\{p^i_{nm}(\mathbf{k})[p^j_{ml}(\mathbf{k})p^k_{ln}(\mathbf{k}) + p^k_{ml}(\mathbf{k})p^j_{ln}(\mathbf{k})]\right\}$ is a symmetrized combination of the transition dipole $\mathbf{p}_{nm} = \langle n\mathbf{k}|\,\hat{\mathbf{p}}\,|m\mathbf{k}\rangle$, $\hbar\omega_{mn}(\mathbf{k}) = \epsilon_m(\mathbf{k}) - \epsilon_n(\mathbf{k})$ is the difference between eigenenergies and $f_{mn}(\mathbf{k}) = f_m(\mathbf{k}) - f_n(\mathbf{k})$ is the difference between occupations of two states in the system. We expect a strong response near the zeros of the demoninator, which – in the energy region under consideration – are given by the two-photon-resonances $\omega_{mn}(\mathbf{k}) - 2\omega = 0$.

Acknowledgement

We are grateful to Karl Unterrainer for providing access to a Ti:Sapphire laser source. We thank Dmitri Nabok for valuable discussions and help on the implementation of the SHG-formulae and Andris Gulans for supplying inputs for the exciting-code. We acknowledge financial support by the Austrian Science Fund FWF (START Y 539-N16 and I 3827-N36),

the European Union (grant agreements No. 785219 and 881603, Graphene Flagship), the doctoral college program "TU-D Unravelling advanced 2D materials" funded by TU Wien, and the IMPRS-APS program of the MPQ (Germany).

Supporting Information Available

The Supporting Information is available free of charge on the ACS Publications website. We give detailed information on computational parameters and extended data for the materials not presented in detail in the main text.

References

(1) Li, Y.; Chernikov, A.; Zhang, X.; Rigosi, A.; Hill, H. M.; van der Zande, A. M.; Chenet, D. A.; Shih, E.-M.; Hone, J.; Heinz, T. F. Measurement of the optical dielectric function of monolayer transition-metal dichalcogenides: MoS2, MoSe2, WS2, and WSe2. *Physical Review B* **2014**, *90*, 205422.

(2) Carvalho, A.; Ribeiro, R. M.; Castro Neto, A. H. Band nesting and the optical response of two-dimensional semiconducting transition metal dichalcogenides. *Physical Review B* **2013**, *88*, 115205.

(3) Gillen, R.; Maultzsch, J. Light-Matter Interactions in Two-Dimensional Transition Metal Dichalcogenides: Dominant Excitonic Transitions in Mono-and Few-Layer MoX _2 and Band Nesting. *IEEE Journal of Selected Topics in Quantum Electronics* **2016**, *23*, 219–230.

(4) Tsuchiya, T. Tensile testing of silicon thin films. *Fatigue & Fracture of Engineering Materials & Structures* **2005**, *28*, 665–674.

(5) Lee, C.; Wei, X.; Kysar, J. W.; Hone, J. Measurement of the elastic properties and intrinsic strength of monolayer graphene. *Science* **2008**, *321*, 385–388.

(6) Roldan, R.; Castellanos-Gomez, A.; Cappelluti, E.; Guinea, F. Strain engineering in semiconducting two-dimensional crystals. *Journal of Physics: Condensed Matter* **2015**, *27*, 313201.

(7) Desai, S. B.; Seol, G.; Kang, J. S.; Fang, H.; Battaglia, C.; Kapadia, R.; Ager, J. W.; Guo, J.; Javey, A. Strain-Induced Indirect to Direct Bandgap Transition in Multilayer WSe2. *Nano Letters* **2014**, *14*, 4592–4597, PMID: 24988370.

(8) Rice, C.; Young, R.; Zan, R.; Bangert, U.; Wolverson, D.; Georgiou, T.; Jalil, R.; Novoselov, K. Raman-scattering measurements and first-principles calculations of strain-induced phonon shifts in monolayer MoS2. *Physical Review B* **2013**, *87*, 081307.

(9) Niehues, I.; Schmidt, R.; Drüppel, M.; Marauhn, P.; Christiansen, D.; Selig, M.; Berghäuser, G.; Wigger, D.; Schneider, R.; Braasch, L. Strain control of exciton–phonon coupling in atomically thin semiconductors. *Nano Letters* **2018**, *18*, 1751–1757.

(10) Levy, N.; Burke, S.; Meaker, K.; Panlasigui, M.; Zettl, A.; Guinea, F.; Neto, A. C.; Crommie, M. Strain-induced pseudo–magnetic fields greater than 300 tesla in graphene nanobubbles. *Science* **2010**, *329*, 544–547.

(11) Castellanos-Gomez, A.; Roldan, R.; Cappelluti, E.; Buscema, M.; Guinea, F.; van der Zant, H. S. J.; Steele, G. A. Local Strain Engineering in Atomically Thin MoS2. *Nano Letters* **2013**, *13*, 5361–5366, PMID: 24083520.

(12) Tonndorf, P.; Schmidt, R.; Schneider, R.; Kern, J.; Buscema, M.; Steele, G. A.; Castellanos-Gomez, A.; van der Zant, H. S. J.; de Vasconcellos, S. M.; Bratschitsch, R. Single-photon emission from localized excitons in an atomically thin semiconductor. *Optica* **2015**, *2*, 347–352.

(13) Srivastava, A.; Sidler, M.; Allain, A. V.; Lembke, D. S.; Kis, A.; Imamoglu, A. Optically active quantum dots in monolayer WSe2. *Nature Nanotechnology* **2015**, *10*, 491 EP –.

(14) He, Y.-M.; Clark, G.; Schaibley, J. R.; He, Y.; Chen, M.-C.; Wei, Y.-J.; Ding, X.; Zhang, Q.; Yao, W.; Xu, X.; Lu, C.-Y.; Pan, J.-W. Single quantum emitters in monolayer semiconductors. *Nature Nanotechnology* **2015**, *10*, 497 EP –.

(15) Koperski, M.; Nogajewski, K.; Arora, A.; Cherkez, V.; Mallet, P.; Veuillen, J.-Y.; Marcus, J.; Kossacki, P.; Potemski, M. Single photon emitters in exfoliated WSe2 structures. *Nature Nanotechnology* **2015**, *10*, 503 EP –.

(16) Chakraborty, C.; Kinnischtzke, L.; Goodfellow, K. M.; Beams, R.; Vamivakas, A. N. Voltage-controlled quantum light from an atomically thin semiconductor. *Nature Nanotechnology* **2015**, *10*, 507 EP –.

(17) Linhart, L.; Paur, M.; Smejkal, V.; Burgdörfer, J.; Mueller, T.; Libisch, F. Localized Intervalley Defect Excitons as Single-Photon Emitters in WSe_2. *Phys. Rev. Lett.* **2019**, *123*, 146401.

(18) Feng, J.; Qian, X.; Huang, C.-W.; Li, J. Strain-engineered artificial atom as a broad-spectrum solar energy funnel. *Nature Photonics* **2012**, *6*, 866.

(19) Peyskens, F.; Chakraborty, C.; Muneeb, M.; Van Thourhout, D.; Englund, D. Integration of Single Photon Emitters in 2D Layered Materials with a Silicon Nitride Photonic Chip. *arXiv preprint arXiv:1904.08841* **2019**,

(20) Frisenda, R.; Drüppel, M.; Schmidt, R.; de Vasconcellos, S. M.; de Lara, D. P.; Bratschitsch, R.; Rohlfing, M.; Castellanos-Gomez, A. Biaxial strain tuning of the optical properties of single-layer transition metal dichalcogenides. *npj 2D Materials and Applications* **2017**, *1*, 10.

(21) He, K.; Poole, C.; Mak, K. F.; Shan, J. Experimental demonstration of continuous electronic structure tuning via strain in atomically thin MoS2. *Nano letters* **2013**, *13*, 2931–2936.

(22) Lloyd, D.; Liu, X.; Christopher, J. W.; Cantley, L.; Wadehra, A.; Kim, B. L.; Goldberg, B. B.; Swan, A. K.; Bunch, J. S. Band gap engineering with ultralarge biaxial strains in suspended monolayer MoS2. *Nano letters* **2016**, *16*, 5836–5841.

(23) Conley, H. J.; Wang, B.; Ziegler, J. I.; Haglund Jr, R. F.; Pantelides, S. T.; Bolotin, K. I. Bandgap engineering of strained monolayer and bilayer MoS2. *Nano letters* **2013**, *13*, 3626–3630.

(24) Mennel, L.; Furchi, M. M.; Wachter, S.; Paur, M.; Polyushkin, D. K.; Mueller, T. Optical imaging of strain in two-dimensional crystals. *Nature Communications* **2018**, *9*, 516.

(25) Mennel, L.; Paur, M.; Mueller, T. Second harmonic generation in strained transition metal dichalcogenide monolayers: MoS2, MoSe2, WS2, and WSe2. *APL Photonics* **2019**, *4*, 034404.

(26) Trolle, M. L.; Seifert, G.; Pedersen, T. G. Theory of excitonic second-harmonic generation in monolayer MoS2. *Physical Review B* **2014**, *89*, 235410.

(27) Leitsmann, R.; Schmidt, W.; Hahn, P.; Bechstedt, F. Second-harmonic polarizability including electron-hole attraction from band-structure theory. *Physical Review B* **2005**, *71*, 195209.

(28) Gulans, A.; Kontur, S.; Meisenbichler, C.; Nabok, D.; Pavone, P.; Rigamonti, S.; Sagmeister, S.; Werner, U.; Draxl, C. Exciting: a full-potential all-electron package implementing density-functional theory and many-body perturbation theory. *Journal of Physics: Condensed Matter* **2014**, *26*, 363202.

(29) Molina-Sánchez, A.; Palummo, M.; Marini, A.; Wirtz, L. Temperature-dependent excitonic effects in the optical properties of single-layer MoS_2. *Phys. Rev. B* **2016**, *93*, 155435.

(30) Louie, S. G.; Rubio, A. *Handbook of materials modeling*; Springer, 2005; pp 215–240.

(31) Fan, Z.; Wei-Bing, Z.; Bi-Yu, T. Electronic structures and elastic properties of monolayer and bilayer transition metal dichalcogenides MX2 (M= Mo, W; X= O, S, Se, Te): a comparative first-principles study. *Chinese Physics B* **2015**, *24*, 097103.

(32) Perdew, J. P.; Burke, K.; Ernzerhof, M. Generalized gradient approximation made simple. *Physical Review Letters* **1996**, *77*, 3865.

(33) Hughes, J. L.; Sipe, J. Calculation of second-order optical response in semiconductors. *Physical Review B* **1996**, *53*, 10751.